



## Article

# Human Nasal Epithelium Organoids for Assessing Neutralizing Antibodies to a Protective SARS-CoV-2 Virus-like Particle Vaccine

Julio Carrera Montoya <sup>1,†</sup>, Simon Collett <sup>1,2,3,†</sup>, Daniel Fernandez Ruiz <sup>1,4</sup>, Linda Earnest <sup>1</sup>, Melissa A. Edeling <sup>1</sup>, Ashley Huey Yiing Yap <sup>1</sup>, Chinn Yi Wong <sup>1</sup>, James P. Cooney <sup>5,6</sup>, Kathryn C. Davidson <sup>5,6</sup>, Jason Roberts <sup>6,7</sup>, Steven Rockman <sup>1,8</sup>, Bang M. Tran <sup>9</sup>, Julie L. McAuley <sup>1</sup>, Georgia Deliyannis <sup>1</sup>, Samantha L. Grimley <sup>1</sup>, Damian F. J. Purcell <sup>1</sup>, Shafagh A. Waters <sup>10,11,12</sup>, Dale I. Godfrey <sup>1</sup>, Dhiraj Hans <sup>13</sup>, Marc Pellegrini <sup>5,6</sup>, Jason M. Mackenzie <sup>1</sup>, Elizabeth Vincan <sup>7,9,14</sup>, William R. Heath <sup>1</sup> and Joseph Torresi <sup>1,\*</sup>

<sup>1</sup> Department of Microbiology and Immunology, University of Melbourne at the Peter Doherty Institute for Infection and Immunity, Melbourne 3010, Australia; julio.carreramontoya@unimelb.edu.au (J.C.M.); s.collett@unimelb.edu.au (S.C.)

<sup>2</sup> Department of Paediatrics, University of Melbourne, Melbourne 3010, Australia

<sup>3</sup> School of Science, College of Science, Engineering and Health, RMIT University, Melbourne 3000, Australia

<sup>4</sup> School of Biomedical Sciences, Faculty of Medicine & Health, the UNSW RNA Institute, The University of New South Wales, Kensington 2052, Australia

<sup>5</sup> Walter and Eliza Hall Institute of Medical Research, Melbourne 3052, Australia

<sup>6</sup> Department of Medical Biology, University of Melbourne, Melbourne 3052, Australia

<sup>7</sup> Victorian Infectious Diseases Reference Laboratory, Doherty Institute for Infection and Immunity, Royal Melbourne Hospital, Melbourne 3052, Australia

<sup>8</sup> Vaccine Innovation Unit, Seqirus, Parkville 3052, Australia

<sup>9</sup> Department of Infectious Diseases, University of Melbourne at the Peter Doherty Institute for Infection and Immunity, Melbourne 3010, Australia

<sup>10</sup> School of Women's and Children's Health, Faculty of Medicine, University of New South Wales, Sydney 2052, Australia

<sup>11</sup> Molecular and Integrative Cystic Fibrosis Research Centre, University of New South Wales, Sydney Children's Hospital, Sydney 2031, Australia

<sup>12</sup> Department of Respiratory Medicine, Sydney Children's Hospital, Sydney 2031, Australia

<sup>13</sup> Research, Innovation & Commercialisation, Faculty of Medicine, Dentistry & Health Sciences, The University of Melbourne, Parkville 3052, Australia

<sup>14</sup> Curtin Medical School, Curtin University, Perth 6102, Australia

\* Correspondence: joseph.torresi@unimelb.edu.au

† These authors contributed equally to this work.



**Citation:** Carrera Montoya, J.; Collett, S.; Fernandez Ruiz, D.; Earnest, L.; Edeling, M.A.; Yap, A.H.Y.; Wong, C.Y.; Cooney, J.P.; Davidson, K.C.; Roberts, J.; et al. Human Nasal Epithelium Organoids for Assessing Neutralizing Antibodies to a Protective SARS-CoV-2 Virus-like Particle Vaccine. *Organoids* **2024**, *3*, 18–31. <https://doi.org/10.3390/organoids3010002>

Academic Editor: Süleyman Ergün

Received: 20 October 2023

Revised: 3 November 2023

Accepted: 19 January 2024

Published: 1 February 2024



**Copyright:** © 2024 by the authors. Licensee MDPI, Basel, Switzerland. This article is an open access article distributed under the terms and conditions of the Creative Commons Attribution (CC BY) license (<https://creativecommons.org/licenses/by/4.0/>).

**Abstract:** Existing mRNA COVID-19 vaccines have shown efficacy in reducing severe cases and fatalities. However, their effectiveness against infection caused by emerging SARS-CoV-2 variants has waned considerably, necessitating the development of variant vaccines. Ideally, next-generation vaccines will be capable of eliciting broader and more sustained immune responses to effectively counteract new variants. Additionally, in vitro assays that more closely represent virus neutralization in humans would greatly assist in the analysis of protective vaccine-induced antibody responses. Here, we present findings from a SARS-CoV-2 VLP vaccine encompassing three key structural proteins: Spike (S), Envelope (E), and Membrane (M). The VLP vaccine effectively produced neutralizing antibodies as determined by surrogate virus neutralization test, and induced virus-specific T-cell responses: predominantly CD4<sup>+</sup>, although CD8<sup>+</sup> T cell responses were detected. T cell responses were more prominent with vaccine delivered with AddaVax compared to vaccine alone. The adjuvanted vaccine was completely protective against live virus challenge in mice. Furthermore, we utilized air-liquid-interface (ALI)-differentiated human nasal epithelium (HNE) as an in vitro system, which authentically models human SARS-CoV-2 infection and neutralization. We show that immune sera from VLP-vaccinated mice completely neutralized SARS-CoV-2 virus infection, demonstrating the potential of ALI-HNE to assess vaccine induced Nab.

**Keywords:** COVID; neutralizing antibody; VLP vaccine; HNE organoids

## 1. Introduction

The COVID-19 pandemic has resulted in devastating loss of lives and immense pressure on healthcare systems globally. The pandemic prompted the rapid development and deployment of several vaccines to curb the spread of the responsible virus, severe acute respiratory syndrome coronavirus 2 (SARS-CoV-2). Among these, the Pfizer-BioNTech BNT162b2 mRNA vaccine demonstrated remarkable efficacy against ancestral SARS-CoV-2 virus. Early clinical trials demonstrated an efficacy of approximately 95% in preventing symptomatic COVID-19 disease [1]. Moderna's mRNA-1273 vaccine also displayed a similar high efficacy of around 94.1% [2]. Both vaccines utilize lipid nanoparticles to deliver stabilized mRNA encoding the spike protein of the SARS-CoV-2 virus, eliciting a robust humoral immune response.

Although these COVID-19 vaccines demonstrated effectiveness in reducing fatalities and severe COVID, their efficacy against the rapidly emerging SARS-CoV-2 viral variants has waned rapidly [3–5]. There is, therefore, a need for the advancement of next-generation COVID-19 vaccines with the ability to generate broader and more durable immune responses, to counteract the emergence of existing and emerging variants.

Most licensed vaccines focus on immunity generated against SARS-CoV-2 Spike (S) protein [6]. Nonetheless, the other three structural proteins, Membrane (M), Nucleoprotein (N) and Envelope (E), are important in producing protective and memory CD4<sup>+</sup> and CD8<sup>+</sup> T cell responses to coronaviruses [7–10]. Thus, the inclusion of these proteins in a vaccine formulation could potentially result in improved vaccine efficacy [11] by producing more potent and broader T cell-based immune responses, in addition to Spike-specific neutralizing antibody (NAb) responses produced by existing COVID-19 vaccines.

VLPs have previously been shown to produce highly effective commercial vaccines, such as Engerix-B<sup>®</sup> (GlaxoSmithKline, Brentford, UK) and Recombivax HB<sup>®</sup> (Merck & Co., Rahway, NJ, USA) against HBV [12,13], Gardasil<sup>®</sup> (Merck & Co.) and Cervarix<sup>®</sup> (GlaxoSmithKline) against HPV [14], Hecolin<sup>®</sup> (Xiamen Innovax Biotech Co., Xiamen, China) against HEV [15,16], and Mosquirix<sup>™</sup> (GlaxoSmithKline Inc.) against malaria [17]. We have previously reported on the application of a novel method to generate VLP vaccines for enveloped RNA viruses, including SARS-CoV-2 [18]. In this study, we examined the use of VLPs produced by expressing individual structural proteins as an approach to developing a SARS-CoV-2 VLP with an interchangeable S protein. The vaccine presented here can be adapted to emerging SARS-CoV-2 variants, and the culmination of these advancements seeks to fortify global responses against the threat of COVID-19.

Here, we present results from a SARS-CoV-2 VLP vaccine comprised of three key structural proteins of SARS-CoV-2—Spike (S), Envelope (E), and Membrane (M)—which contribute to both protective B cell (antibody), and memory CD4<sup>+</sup> and CD8<sup>+</sup> T cell responses [7,8,10]. Mouse immunization studies showed that this vaccine produced neutralizing antibody (Nab), together with SARS-CoV-2-specific T-cell responses, and that the induced immunity was fully protective in mice against challenge with live SARS-CoV-2 virus.

Culture systems, such as air–liquid-interface (ALI)-differentiated human nasal epithelium (HNE), present a novel model of SARS-CoV-2 infection in the upper respiratory tract, the predominant site for viral infection and replication [19]. We tested the ability of sera from mice immunized with our SARS-CoV-2 VLP vaccine adjuvanted with AddaVax to neutralize SARS-CoV-2 *in vitro* in ALI-HNE cultures, and demonstrated complete virus neutralization against homologous strain virus, compared to sera from unvaccinated mice.

## 2. Materials and Methods

### 2.1. Cells

Vero cells (African Green Monkey Kidney, clone CCL-81) and HEK293T cells (human embryonic kidney 293T) were maintained in Dulbecco's Modified Eagle Medium (DMEM) (Gibco™ #11995073, Waltham, MA, USA) supplemented with 10% fetal bovine serum (FBS) and 1% Glutamax (Gibco™ #35050061, Waltham, MA, USA), unless differently stated. For VLP production, Vero cells were initially gradually adapted to grow in low FBS conditions (1–2%) or serum free medium (SFM) [18].

### 2.2. VLP Production and Purification

The sequence used for the generation of the construct was based on sequence NC\_045512.2. Production of Ancestral-SARS-CoV-2 VLPs was as previously described [18]. In brief, individual recombinant Spike (S), Envelope (E) and Membrane (M) Adenovirus vectors were produced using the AdEasy Adenoviral Vector System (Agilent, Santa Clara, CA, USA). Each viral gene was amplified individually from a single codon optimized SEM genetic construct by PCR cloning; the forward primers were designed to introduce a *KpnI* enzyme restriction site followed by a Kozak sequence and a start codon. The reverse primers were designed to amplify from the 5' end of each viral gene, introducing a stop codon and a *NotI* restriction site (Table S1).

After amplification and digestion with *KpnI* and *NotI* enzymes, DNA was cloned into a pAdTrack-CMV cloning vector, linearized with *PmeI* enzyme, and co-transformed with the pAdEasy-1 plasmid (in BJ5183-AD-1 cells) by homologous recombination, and then re-transformed into Top10F' cells for stable plasmid propagation. Clones were confirmed by Sanger sequencing (Australian Genome Research Facility—AGRF). The pAdTrackCMV-pAdEasy1 plasmids containing the target sequences were then linearized with *PacI* restriction enzyme, ethanol precipitated and resuspended in sterile water. Four micrograms of digested plasmid were transfected into 10 cm dishes of HEK293T cells for Adenovirus-vector production and subsequent amplification by serial passaging into the same cell line.

Once high titer viral stocks had been produced, the individual S, E, and M Adenovirus vectors were used to infect Vero cells grown in 5-layer T875 flasks, as previously described [18]. Each of the Adenovirus vectors (S, E, and M) was added at the same time in an MOI of 1.0 in a total of 4 mL of medium per layer. The next day, cells were washed three times with PBS to remove excess adenovirus vector and incubated for 5 more days. SARS-CoV-2 VLPs were harvested from culture supernatants and purified by ultracentrifugation as previously described. SARS-CoV-2 VLP concentration was measured by Bradford assay, according to the manufacturer's instructions (Coomassie Plus Bradford Protein Assay, Thermo Fisher Scientific #23236, Waltham, MA, USA).

### 2.3. Direct-VLP Enzyme-Linked Immunosorbent Assay (ELISA)

The presence of SARS-CoV-2 spike and receptor binding domain (RBD) on purified VLPs was confirmed by coating 96-well, flexible, flat-bottomed PVC microtiter plates (Nunc, Thermo Fisher Scientific #442404) with 50 µL of VLP (20 µg/mL) in PBS and incubated overnight at 4 °C. Coating solution was then discarded and wells were blocked with blocking buffer (2% BSA in PBS) and incubated for 1 h at 37 °C. Plates were then washed 4 times with PBS supplemented with 0.05% Tween and blotted dry. Primary antibody (anti-Spike polyclonal rabbit antibody, Sinobiological #40591-T62, or anti-SARS-CoV-2 RBD polyclonal rabbit antibody, My BioSource #MBS2563840, San Diego, CA, USA) or mouse-serum was added in two-fold serial dilutions in blocking buffer from 1 in 800 down to 1 in 102,400. Fifty microliters of the diluted antibody were added to the appropriate wells and plates incubated for 1 h at 37 °C. Plates were then washed again four times with PBST 0.05%, and 50 µL of goat anti-rabbit secondary antibody conjugated to horseradish peroxidase (HRP) (Dako #P0448, Santa Clara, CA, USA) at 1/2500 was made up in blocking buffer and added to each well. After incubation for 1 h at room temperature, plates were washed again with PBST 0.05% and blotted dry. A total of 50 µL of tetramethylbenzidine (TMB) substrate (Thermo Fisher Scientific #002023) was added to each well and incubated

for 10 to 15 min at room temperature, before stopping the reaction by adding 50  $\mu\text{L}$ /well of 0.16 M  $\text{H}_2\text{SO}_4$ . Absorbance values were determined on a Labsystems Multiskan Multisoft plate reader (Thermo Fisher Scientific) at 450 nm.

#### 2.4. Negative Staining by Transmission Electron Microscopy (TEM)

For negative staining and subsequent TEM examination, 6  $\mu\text{L}$  of VLP containing suspension or SARS-CoV-2 AUS/VIC01/2020 control material were applied directly to a glow-discharged 400-mesh copper formvar-carbon coated grid and allowed to adsorb for 20 s. The suspension was removed by blotting, and then negative stained using 3% phosphotungstic acid (pH 7.0). The negative-stained grids were blotted to remove excess stain and air-dried at room temperature.

Negative stained samples were examined using an FEI Tecnai T12 Spirit electron microscope (Tecnai, Hillsboro, OR, USA) operating at an acceleration voltage of 80 kV. Electron micrographs were collected using an FEI Eagle 4k CCD camera (FEI, Hillsboro, OR, USA). File type conversion and morphometry were performed using the FEI TIA software package (V18).

#### 2.5. Mice and Vaccinations

Mice were bred in-house at the Peter Doherty Institute for Infection and Immunity, Biological Research Facility, Melbourne, Australia. Female C57BL/6 mice, 6–10 weeks old, were used for immunization with Ancestral-SARS-CoV-2 VLPs. For the live virus challenge, mice were vaccinated at days 0 and 14 with PBS (negative control), 20  $\mu\text{g}$  of SARS-CoV-2 VLPs, or with 20  $\mu\text{g}$  SARS-CoV-2 VLP with AddaVax (1:1 *v/v*), all in a total volume of 50  $\mu\text{L}$ . Bleeds were taken at day 0, 14, 28 and 42. At day 45, mice were challenged with SARS-CoV-2 N501Y + D614G virus, and at day 48 euthanized for spleen harvest. SARS-CoV-2 N501Y + D614G virus naturally arose as a clinical isolate from the clinical isolate hCoV-19/Australia/VIC2089/2020. SARS-CoV-2 infection was performed using an inhalation exposure system (Glas-Col, LLC, Terre Haute, IN, USA) loaded with  $1.5 \times 10^7$  SARS-CoV-2 TCID<sub>50</sub>. Briefly, animals were placed in compartmented mesh baskets within the chamber of a Glas-Col Inhalation Exposure System and exposed to nebulized SARS-CoV-2 N501Y + D614G strain virus for 30 min. All procedures involving animals and live SARS-CoV-2 were conducted in an OGTR-approved Physical Containment Level 3 (PC3) facility at the Walter and Eliza Hall Institute of Medical Research (Cert-3621), and were approved by The Walter and Eliza Hall Institute of Medical Research Animal Ethics Committee (2020.016).

For T-cell experiments, mice were injected with 1, 2 or 3 doses of 10  $\mu\text{g}$  Ancestral-SARS-CoV-2 VLP formulated with AddaVax (1:1 *v/v*), 14 days apart. An additional group received 2 doses of 5  $\mu\text{g}$  SARS-CoV-2 VLP on days 0 and 14. Mice injected with PBS three times were used as controls. Mice were euthanized on day 42, and splenocytes ( $2 \times 10^5$  per well) were restimulated *in vitro* using primary dendritic cells (DC) ( $10^5$  per well) derived from naïve C57BL/6 mice, pre-cultured with 5  $\mu\text{g}$ /well VLP or not. Mice were routinely monitored, including weight, and were euthanized before signs of disease or infection.

All procedures were approved by the University of Melbourne Animal Ethics Committee (2020-20198).

#### 2.6. Measurement of Viral Loads via 50% Tissue Culture Infectious Dose (TCID<sub>50</sub>)

TCID<sub>50</sub> was performed as previously described [20]. Briefly, African green monkey kidney epithelial Vero cells, purchased from ATCC (clone CCL-81), were seeded in flat-bottom 96-well plates ( $1.75 \times 10^4$  cells/well) and left to adhere overnight at 37 °C, 5% CO<sub>2</sub>. Cells were washed twice with PBS and transferred to serum-free DMEM containing TPCK trypsin (0.5  $\mu\text{g}/\text{mL}$  working concentration). Infected organs were defrosted, homogenized, clarified by centrifugation at  $10,000 \times g$  for 5 min at 4 °C, and supernatant was added to the first row of cells at a ratio of 1:7, followed by 9 rounds of 1:7 serial dilutions in the other rows. Cells were incubated at 37 °C, 5% CO<sub>2</sub> for 4 days, until virus-induced cytopathic effect (CPE) was scored. TCID<sub>50</sub> was calculated using the Spearman and Kärber algorithm.

### 2.7. SARS-CoV-2 Surrogate Virus Neutralization Test (sVNT) Assays

Assays were performed using an sVNT Kit (GenScript #L00847-A, Piscataway, NJ, USA) following the manufacturer's protocol. Percentage of inhibition was calculated according to the following formula:

$$\% \text{ of inhibition} = 1 - \frac{\text{OD value of sample}}{\text{OD value of negative control}} \times 100\%$$

### 2.8. ALI-HNE Organoids

Researchers received de-identified, cryopreserved human nasal epithelium basal cells generated under conditional reprogram conditions, as previously described [21], from the Molecular and Integrative Cystic Fibrosis Research Centre (miCF RC), University of New South Wales, New South Wales, Australia. The basal progenitors (donor PDI-1, [19]) were thawed and seeded onto collagen-coated (PureCol-S, Advanced BioMatrix, San Diego, CA, USA) Transwell inserts (6.5 mm Corning, Kennebunk, ME, USA) and cultured submerged in PneumaCult™ ExPlus (STEMCELL Technologies, Vancouver, BC, Canada) until confluent, typically 4–7 days, and then switched to PneumaCult™ ALI medium (STEMCELL Technologies) for 2–3 days. Mucociliary differentiation at ALI was initiated by removing the apical medium and exposing the cells to air. The basal medium was replaced 3 times a week for 3–4 weeks, and mucocilliary differentiation monitored microscopically to detect beating cilia and mucous production, as we described [19].

Study approval was received from the Sydney Children's Hospital Network Ethics Review Board (HREC/16/SCHN/120) and the Medicine and Dentistry Human Ethics Sub-Committee, University of Melbourne (HREC/2057111). Written consent was obtained from all participants (or participants' guardians) prior to collection of biospecimens.

### 2.9. SARS-CoV-2 Propagation and ALI-HNE Infection

Human SARS-CoV-2 clinical isolates BetaCoV/Australia/VIC01/2020 (referred to as VIC01) were propagated on Vero cells (ATCC) in DMEM (Gibco), as previously described [19]. To infect ALI-HNE with SARS-CoV-2, organoid cultures were incubated with either (a) no virus (mock), (b) live virus (VIC01), live virus pre-incubated with serum from mice injected with either (c) PBS or (d) VLP vaccine formulated with AddaVax, and (e) virus pre-incubated with Nab [22]. The corresponding inoculum was added to the apical surface at an MOI of 0.02 or 0.002 in 30 µL (assuming ~300,000 cell at the ALI-HNE surface). After adsorption for 2 h at 37 °C, the inoculum was washed off with PBS containing calcium and magnesium chloride (PBS++). Two hundred microliters of PBS++ was then added to the apical surface and harvested after 10 min at 37 °C, before being stored at –80 °C. Apical PBS++ washes were harvested in the same way at the indicated time points. Apical PBS++ wash samples, and basal medium collected at time of medium change, and were assayed for infectious virus by TCID<sub>50</sub> as above.

### 2.10. Immunofluorescence and Confocal Microscopy

Cells from ALI-HNE organoids were fixed, permeabilized, blocked, and stained, as previously described [19]. The primary antibodies used for immunofluorescence include acetylated α-tubulin (Sigma-Aldrich #T7451, St. Louis, MO, USA; 1:250 dilution) and SARS Nucleocapsid protein (Novus Biologicals #NB100-56683, Centennial, CO, USA; 1:200 dilution). The secondary antibodies used for immunofluorescence include goat anti-mouse Alexa Fluor 488 (Invitrogen #A11001, Waltham, MA, USA; 1:450 dilution) and goat anti-rabbit Alexa Fluor 647 (Invitrogen #A21244, 1:450 dilution). The confocal microscopy imaging was acquired on the Zeiss LSM 780 system (Oberkochen, Baden-Württemberg, Germany). The acquired Z-sections were stacked and processed using ImageJ software (NIH, Bethesda, MD, USA, Fiji 2.15).

### 2.11. ELISpot

First, 0.45  $\mu\text{m}$  MultiScreen-IP sterile, clear Filter Plates (Merck) were coated overnight with 3 mg/mL IFN- $\gamma$  capture Ab (clone AN-18; WEHI Antibody Services) in PBS and blocked with RPMI containing 10% fetal calf serum (FCS) for 30 min at RT. Then,  $2 \times 10^5$  splenocytes/well from immunized mice (either depleted of CD4 $^+$  or CD8 $^+$  T cells, or non-depleted) were plated and cultured for 20 h at 37  $^\circ\text{C}$  and 5% CO $_2$  in a humidified incubator in the presence or absence of  $10^5$  primary DC enriched from spleens of DC donor mice (see below) and VLP. Concanavalin A (5 mg/mL) was used as positive control. Plates were then incubated for 2 h with 1 mg/mL biotin-conjugated IFN- $\gamma$  detection mAb (clone R4-6A2; WEHI Antibody Services), and diluted in PBS containing 0.5% FCS, followed by incubation with Streptavidin-HRP (MabTech, Stockholm, Sweden) for 1 h at RT and with TMB substrate for 15 min. Plates were washed after each incubation step. An AID ELISpot reader (Advanced Imaging Devices GmbH, Strassberg, Germany) was used to enumerate spots. In vitro depletion of CD4 $^+$  and CD8 $^+$  T cells was achieved by incubation of splenocytes with a CD4 mAb (clone GK1.5) or a CD8 mAb (clone 5.3-67) for 30 min, followed by incubation with BioMag beads for 10 min at 4  $^\circ\text{C}$ , in constant rotation. Control non-depleted splenocytes in the in vitro T cell depletion experiments were also incubated with BioMag beads for consistency.

### 2.12. Isolation of Primary Dendritic Cells

Dendritic cells were isolated from the spleens of naïve mice, or mice treated with FMS-like tyrosine kinase 3 receptor ligand (Flt3-L)-producing cells, in which case Flt3-L was given by subcutaneous injection of  $10^6$  Flt3-L-expressing B6 myeloma cells [23], as previously described [24]: Spleens of donor mice were finely minced and digested in 1 mg/mL collagenase 3 (Worthington Biochemical Corporation, Lakewood, NJ, USA) and 20  $\mu\text{g}/\text{mL}$  DNase I (Roche Diagnostics, Mannheim, Germany) under intermittent agitation for 20 min at room temperature. DC-T cell complexes were then disrupted by adding EDTA (pH 7.2) to the digest to a final concentration of 7.9 mM and continuing the incubation for an additional 5 min. After removing undigested fragments by filtering through a 70  $\mu\text{m}$  mesh, cells were resuspended in 5 mL of 1.077 g/cm $^3$  isosmotic nycodenz medium (Nycomed Pharma AS, Oslo, Norway), layered over 5 mL nycodenz medium, overlaid with 1–2 mL FCS, then centrifuged at  $1700 \times g$  at 4  $^\circ\text{C}$  for 12 min. DC were resuspended in complete RPMI medium supplemented with 10% FCS before use in functional assays.

## 3. Results

### 3.1. SARS-CoV-2 VLPs Exhibit Reactivity for Spike Protein and RBD

To show that our produced VLPs were assembled and produced to the same antigenic authenticity as the wild-type virus we assessed their reactivity to spike-specific antibodies by ELISA and assessed the VLP morphology by EM (Figure 1). We observed that the ELISA assays with SARS-CoV-2 VLPs coated on plates showed strong reactivity of the S protein and its RBD using Ancestral anti-spike and anti-RBD specific antibodies (Figure 1A,B). This confirmed that expression of the S, E, and M containing VLPs presented spike protein that preserves neutralizing S-epitopes on the surface of the virion. Negative staining and TEM analysis showed that the VLPs assembled as pleomorphic spherical particles of approximately 70–100 nm in diameter surrounded by characteristic spike protein (Figure 1(Ci,Cii)). Fixed SARS-CoV-2 virus particles were used as a positive control and show a typical virus particle surrounded by spike protein (Figure 1(Ciii)).

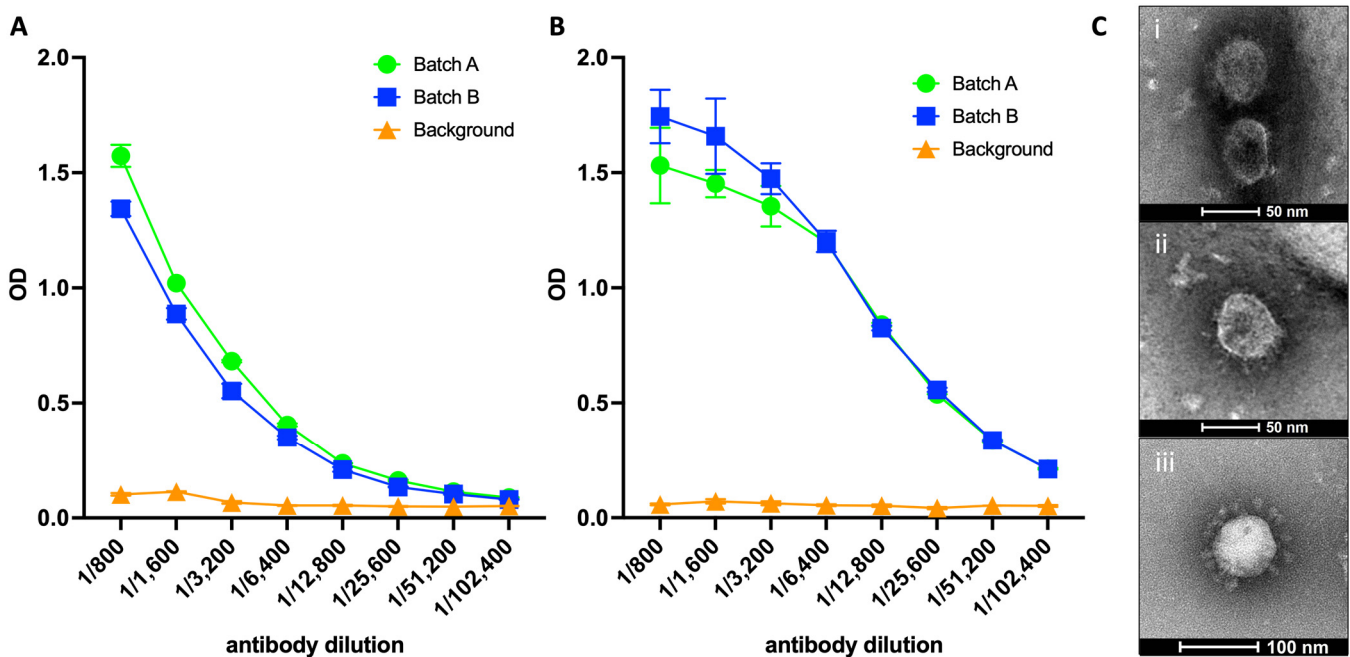


**Figure 1.** Characterization of Ancestral-SARS-CoV-2 VLPs. 20  $\mu\text{g}/\text{mL}$  of two batches of ancestral-SARS-CoV-2 VLPs were analyzed for the presence of (A) Ancestral-SARS-CoV-2 Spike protein (detected with polyclonal antibody Sinobiological #40591-T62), and (B) RBD (detected with polyclonal antibody My BioSource #MBS2563840) on Ancestral-SARS-CoV-2 VLPs as determined by ELISA. Plates were coated with VLPs and probed with either anti Spike or anti-RBD antibody in 2-fold dilutions from 1:800 to 1:102,400 (mean  $\pm$  SD). (C) Morphology of Ancestral-SARS-CoV-2 VLPs (i,ii) and SARS-CoV-2 (iii) as confirmed by EM imaging.

### 3.2. SARS-CoV-2 VLPs Induce Nab Responses and Completely Protect against Viral Challenge

To investigate the immunogenicity and efficacy of our VLP vaccine, we vaccinated mice with two doses of 20  $\mu\text{g}$  of Ancestral-SARS-CoV-2 VLPs delivered with or without AddaVax adjuvant, two weeks apart. We then challenged vaccinated mice with the mouse-adapted N501Y + D614G SARS-CoV-2 strain on day 42 after the first vaccination. ELISA assays using serum from immunized mice also showed strong antigenicity (OD > 1 Spike and >0.6 RBD, Figure S1). To assess the protective effect of the VLPs, we performed a TCID<sub>50</sub> assay of the virus recovered from the lungs of challenged mice and observed 100% protection against live virus in the immunized group (Figure 2A). Nab responses were further investigated by performing SARS-CoV-2 Surrogate Virus Neutralization Test sVNT assays with sera from immunized mice. Inhibition of binding of SARS-CoV-2 ancestral RBD to human ACE2 with the immune sera from mice immunized with isogenic SARS-CoV-2 VLPs with AddaVax ranged from 38% to 78% (Figure 2B) and correlated with protection against viral challenge in the same vaccine group (Figure 2A). Considerable variation was seen between mice in both TCID<sub>50</sub> values, in the group that received VLP vaccine without adjuvant, and inhibition, as measured by sVNT assay, in the mice that received vaccine with and without adjuvant. However, complete protection was seen in mice receiving the VLP vaccine with adjuvant, highlighting the importance of delivery of the vaccine with an adjuvant.

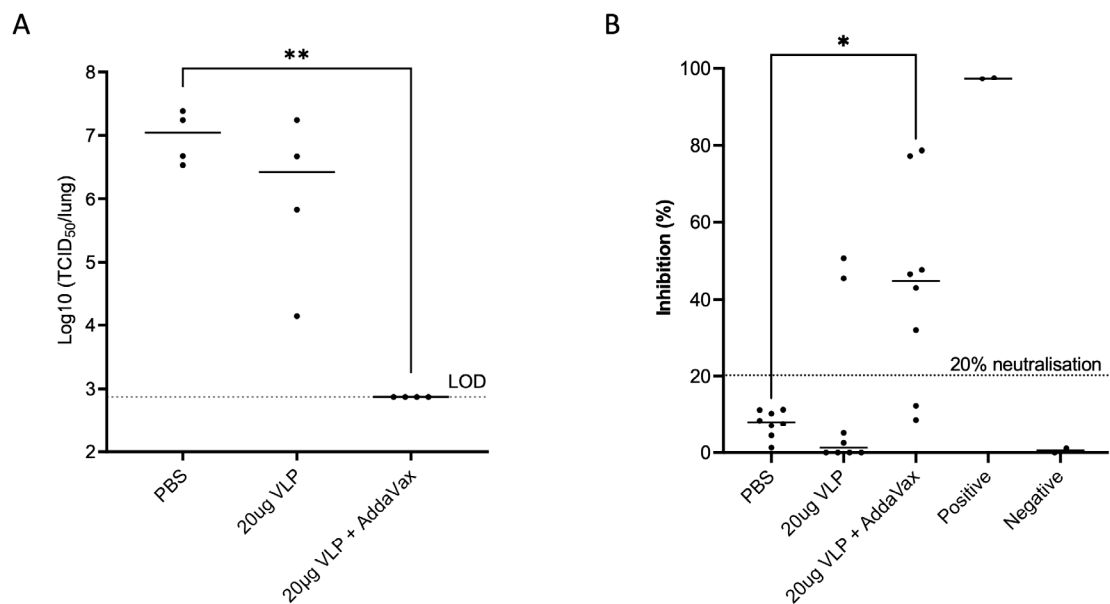


**Figure 2.** Determination of protection in a mouse model after immunization with Ancestral-SARS-CoV-2 VLPs. **(A)** TCID<sub>50</sub> values from lungs of four mice per group immunized with PBS, 20 µg of VLP or 20 µg of Ancestral-SARS-CoV-2 VLP with AddaVax, and then challenged with live SARS-CoV-2 virus VIC2089(N501Y). **(B)** sVNT assay performed on sera from mice immunized with either 20 µg Ancestral-SARS-CoV-2 VLPs alone or formulated with AddaVax, or PBS only. Data were analyzed using non-parametric one-way ANOVA test on ranks—Kruskal–Wallis test (\*  $p < 0.05$ , \*\*  $p < 0.01$ ). Bar indicates mean value; each dot represents one mouse. Data are from a single immunization experiment.

### 3.3. Mouse Sera from VLP Vaccinated Mice Completely Neutralizes SARS-CoV-2 Virus in an ALI-HNE Model

We have previously shown that ALI-HNE provides a robust cell culture model for SARS-CoV-2 infection [19]. We therefore utilized this cell culture system to further investigate the neutralizing capacity of sera from mice immunized with our VLP vaccine in a human model of virus neutralization more physiologically relevant than monolayer cultures of single cell types. The SARS-CoV-2-VIC01 isolate was used to infect organoid cultures pre-incubated with serum from mice injected with either PBS or with SARS-CoV-2 VLP vaccine formulated with AddaVax. Mock infections with media alone, and infection with virus alone and virus pre-incubated with a known Nab [22], were performed as infectivity controls and positive neutralization controls. We observed significant staining for SARS-CoV-2 NP in the VIC01 only and VIC01 + PBS samples indicating robust infection of the ALI cultures (Figure 3A). Importantly, no SARS-CoV-2 nucleoprotein was detected in the VIC01 + VLP/Ad infected cultures indicating complete neutralization of infection with the sera from mice immunized with isogenic Ancestral-SARS-CoV-2 VLPs with AddaVax (Figure 3A). The absence of SARS-CoV-2 detected in the VIC01 + VLP/Ad infected cultures was analogous to that observed for VIC01 + Nab and mock-infected cultures (Figure 3A). This finding was supported quantitatively by the calculation of TCID<sub>50</sub> values from infected cultures, where serum from mice vaccinated with 20 µg Ancestral-SARS-CoV-2 VLPs with AddaVax showed complete neutralization of virus in the organoid culture, similar to mock infection and neutralization with the positive control neutralizing mouse antibody [22]. In contrast, serum from mice injected with PBS did not neutralize the virus (Figure 3B).

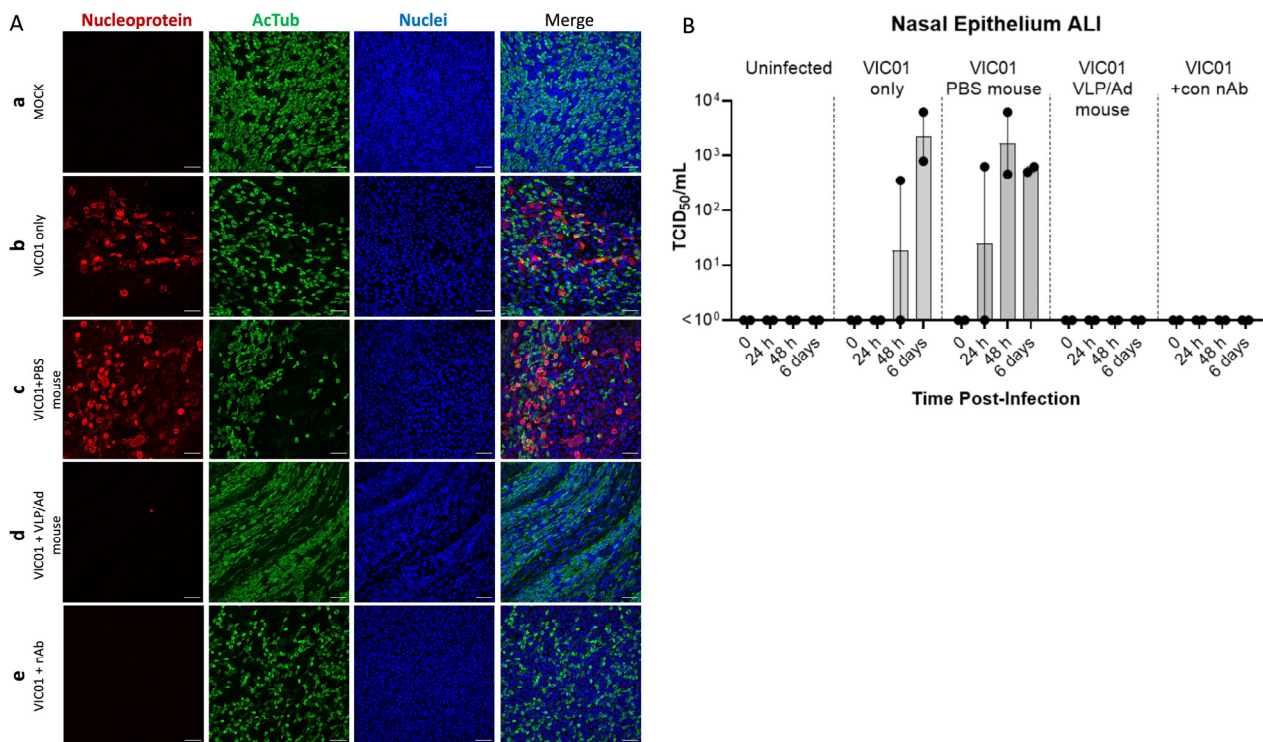


**Figure 3.** Neutralization of SARS-CoV-2 VIC01 in ALI-HNE organoid cultures. (A) Organoid cultures were incubated with either (a) no virus (mock), (b) live virus (VIC01), live virus pre-incubated with serum from mice injected with either (c) PBS or (d) 20  $\mu$ g of VLP vaccine formulated with AddaVax, and (e) virus pre-incubated with neutralizing antibody [22]. Organoid cultures were then stained for SARS-CoV-2 nucleoprotein (red), acetylated  $\alpha$ -tubulin (AcTub) (green) and nuclear DNA (DAPI) (blue). Scale bar is 50  $\mu$ m. (B) TCID<sub>50</sub> values determined from apical wash of organoid cultures ( $n = 2$  for each time point and condition).

### 3.4. T Cells Play a Role in Response against SARS-CoV-2 after Vaccination

We next sought to determine whether our Ancestral-SARS-CoV-2 VLP vaccine elicited measurable T-cell responses in mice. Mice (4–5 per group) were vaccinated intramuscularly with 1–3 doses of Ancestral-SARS-CoV-2 VLP formulated with AddaVax, 2 weeks apart. The number of IFN- $\gamma$ -producing cells in the spleens of these mice were then measured by ELISpot on day 42 (Figure 4A). While addition of antigen (VLP) to the dendritic cells (DC) slightly increased background responses in non-immunized mice (Figure 4A, group A, Spl + DC + VLP vs. Spl + DC), splenocytes from vaccinated mice incubated with DC and SARS-CoV-2 VLP displayed a clearly distinguishable response compared to splenocytes from non-immunized mice (Figure 4A, groups B–E vs. A, Spl + DC + VLP), and this was also reflected in the extrapolated total number of responding cells per spleen (Figure 4B). Interestingly, no differences were detected among vaccinated mice despite varying number of vaccine doses (1 vs. 3, Figure 4A, groups B–D, Spl + DC + VLP, Figure 4B) or amount of SARS-CoV-2 VLP per dose (5  $\mu$ g vs. 10  $\mu$ g VLP/dose, Figure 4A, groups C vs. E, Spl + DC + VLP, Figure 4B). All splenocytes responded equivalently to Concanavalin A (Supplementary Figure S2A). Next, we vaccinated mice twice, 2 weeks apart, with 10  $\mu$ g VLP/dose in the presence or absence of AddaVax. Mice were euthanized one week after the last vaccine dose and their splenocytes assessed for their capacity to respond to Ancestral-SARS-CoV-2 VLP using ELISpot. Again, a clear response was detected by splenocytes from Ancestral-SARS-CoV-2 VLP/AddaVax vaccinated mice, in contrast to those from Ancestral-SARS-CoV-2 VLP-only or unvaccinated mice (Figure 4C,D, Supplementary Figure S2B).

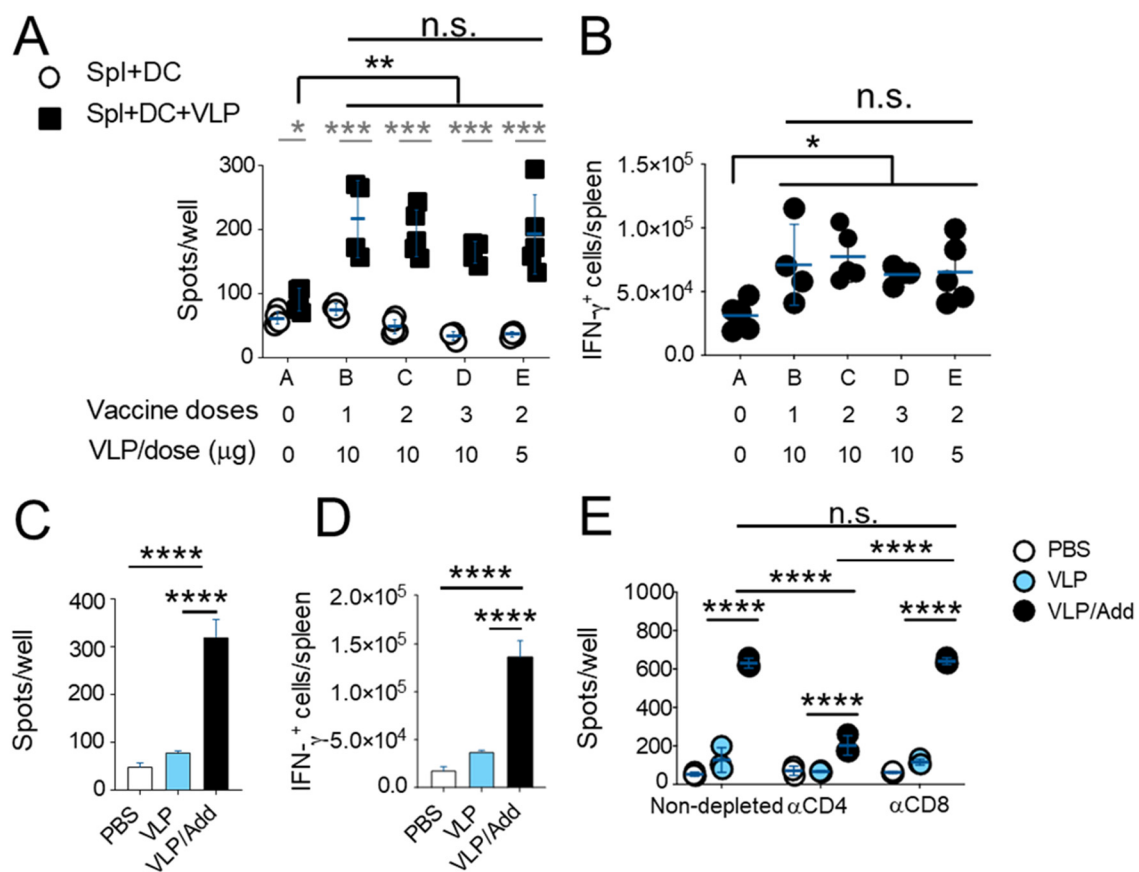


**Figure 4.** Detection of T cell responses elicited by the Ancestral-SARS-CoV-2 VLP vaccine formulated with AddaVax. **(A)** C57BL/6 mice were injected with 1, 2 or 3 doses of 10  $\mu\text{g}$  Ancestral-SARS-CoV-2 VLP formulated with AddaVax (1:1 *v/v*) 14 days apart. An additional group received 2 doses of 5  $\mu\text{g}$  VLP on days 0 and 14. Mice injected with PBS thrice were used as controls. Numbers of IFN- $\gamma$ -producing cells were measured using ELISpot. Data were log-transformed and compared using t-test (to compare Spl + DC vs. Spl + DC + VLP—grey bars and asterisks) or One-Way ANOVA and Tukey’s Multiple Comparisons test (to compare Spl + DC + VLP among different groups—black bars and asterisks). n.s. = not significant; all groups under this bar (**B–E**) were compared to each other. **(B)** Numbers of responding cells/well (i.e., per  $2 \times 10^5$  splenocytes) were extrapolated to the total number of splenocytes per mouse. Data were log transformed and compared using One-Way ANOVA and Tukey’s Multiple Comparisons test. Data in **A** and **B** are from a single immunization experiment with 4–5 mice/group. Each dot represents a sample from a single mouse. Blue lines denote Mean  $\pm$  SD. **(C)** and **(D)** Mice were injected with 2 doses of 10  $\mu\text{g}$  VLP, *i.m.*, formulated or not with AddaVax 14 days apart. Control mice received PBS. Numbers of IFN- $\gamma$ -producing cells were measured using ELISpot. All spleens in each group ( $n = 3$ ) were pooled and analyzed in triplicate wells per group. Data are from a single immunization experiment and were analyzed using one-way ANOVA. Error bars denote SD. Data in **(C)** and **(D)** reflect the number of spots/well and average total number of responding splenocytes per mouse, respectively. **(E)** Mice were vaccinated and splenocytes extracted, restimulated with VLP *in vitro*, and screened for IFN- $\gamma$  production using ELISpot as in **C**, but CD4<sup>+</sup> or CD8<sup>+</sup> T cells were depleted prior to culture using magnetic beads mixed with anti-CD4 and anti-CD8 antibodies. Non-depleted samples were incubated with beads without antibodies. Data are from a single immunization experiment and were analyzed using one-way ANOVA (\*  $p < 0.05$ , \*\*  $p < 0.01$ , \*\*\*  $p < 0.001$ , \*\*\*\*  $p < 0.0001$ ). Blue lines denote mean  $\pm$  SD.

We next sought to determine the contribution of CD4<sup>+</sup> and CD8<sup>+</sup> T cells to the observed responses induced by the vaccine. To do this, we magnetically depleted either CD4<sup>+</sup> or CD8<sup>+</sup> T cells (Supplementary Figure S2C) from cell suspensions prepared from the spleens

of mice vaccinated twice with 10 µg VLP and measured their IFN-γ responses to Ancestral-SARS-CoV-2 VLP using ELISpot (Figure 4E, Supplementary Figure S2D). While depletion of CD8<sup>+</sup> T cells had no detectable effect on the size of the IFN-γ response to SARS-CoV-2 VLP, CD4<sup>+</sup> T cell depletion reduced the frequency of spots to near background levels (Figure 4E). These observations indicate that CD4<sup>+</sup> T cells were major contributors to the response elicited by SARS-CoV-2 VLP vaccination.

#### 4. Discussion

We have previously shown SARS-CoV-2 VLPs can be generated from a single gene sequence encoding the S, M, and E proteins of SARS-CoV-2, with engineered sites for self-cleavage between each protein and are strongly immunogenic [18]. Here, we present data from a SARS-CoV-2 VLP-based vaccine candidate developed using individual expression cassettes of ancestral SARS-CoV-2 S, E, and M structural proteins. These Ancestral-SARS-CoV-2 VLPs contained spike protein trimers with ancestral RBD, and self-assembled into pleomorphic spherical particles of approximately 70–100 nm displaying characteristic spikes on the surface (Figure 1C). The purpose of the approach described herein over our previously described polypeptide approach [19] was to assess the feasibility of swapping an interchangeable S protein into the production steps to allow for the rapid development of vaccines against emerging SARS-CoV-2 variants. Using this VLP platform, we have demonstrated that mice inoculated with the Ancestral-SARS-CoV-2 VLPs were afforded complete protection from infection by live ancestral SARS-CoV-2 virus.

Protection in mice in part corresponds to circulating Nab titers. We therefore wanted to show the neutralizing capacity of sera from inoculated mice in a cell culture system that should have greater relevance to virus neutralization in humans. We have previously shown that VLPs interact differently with cells grown in monolayer cultures compared with 3-dimensional organoid cultures [25]. The HNE-ALI system also provides the capacity for growing virus in an in vitro system that closely recapitulates the in vivo infection site [19], and could therefore become an important model for neutralization assays and the study of the viral infection kinetics of emerging SARS-CoV-2 variants. We therefore explored the use of the HNE-ALI system to show virus neutralization by Ancestral-SARS-CoV-2 VLP vaccine induced Nabs in this model.

Complete protection from infection in both a mouse challenge study and a primary human nasal endothelium organoid culture model was observed, despite less than 100% neutralization being seen by sVNT assay. These observations would suggest that our VLP vaccine might be protective via mechanisms beyond the generation of Nab targeting the RBD. These mechanisms could involve antibodies that target different parts of S or the other structural proteins contained in the VLPs, or Fc dependent non-neutralizing antibodies [26,27].

In addition to humoral responses, the development of robust T cell responses has been shown to be important in protection from, and clearance of, SARS-CoV-2 virus [9–12]. Furthermore, differences are seen in the magnitude of CD4<sup>+</sup> and CD8<sup>+</sup> T cell responses. Various studies have shown CD4<sup>+</sup> T cells to be more important than CD8<sup>+</sup> T cells in the clearance of SARS-CoV-2 [7,8,10,28]. We therefore asked if the Ancestral-SARS-CoV-2 VLPs can produce T cell responses and, if so, whether they are predominantly CD4<sup>+</sup> or CD8<sup>+</sup> T cell responses. Interestingly, findings from the T cell depletion studies highlight the potential contribution of both CD4<sup>+</sup> and, to a lesser degree, CD8<sup>+</sup> T cell responses to an effective and protective immune response produced by the vaccine. Similar investigations of the contribution of T cell mediated protection elicited by newly developed vaccines against SARS-CoV-2 variants are currently in progress.

In this study, we used individual adenoviruses to deliver S, M, and E proteins to produce our VLPs to determine the feasibility of being able to change different components of the VLPs, thereby creating a more adaptable platform. The individual design enables targeted updates to individual genes, in particular the S gene, when necessary. However, from a commercial standpoint, this attribute has limitations due to the need for separate

production of adenoviral vectors, leading to increased expense and process complexity. To address this challenge, we previously developed a self-cleaving sequence to streamline gene expression within a single plasmid construct and to avoid the reliance on multiple adenovirus vectors [18]. A combination of a self-cleaving construct with a separate interchangeable adenovirus to express variant S proteins of emerging viruses would create a more flexible approach for the rapid production of VLP based variant vaccines.

## 5. Conclusions

We present here a system for the generation of SARS-CoV-2 VLPs that would allow for the genes encoding the structural proteins to be easily updated as need dictates. Further, we have shown these VLPs to be protective in mouse and cell culture models. The results presented here indicate that mechanisms of protection other than RBD specific neutralizing antibodies responses may be involved in the protection generated by this vaccine, paving the way for other SARS-CoV-2 variant-specific VLP vaccines. Further work on this promising VLP vaccine platform is ongoing in our laboratory. This includes more detailed T cell studies using Beta, Omicron BA.5 and EG.5 SARS-CoV-2 VLPs, which we are progressing to manufacturing and later to clinical trials.

**Supplementary Materials:** The following supporting information can be downloaded at: <https://www.mdpi.com/article/10.3390/organoids3010002/s1>, Figure S1: Direct Ancestral-SARS-CoV-2 VLP and anti-RBD ELISA; Figure S2: Splenocyte stimulation positive controls and T cell depletion efficiencies; Table S1: Primers used to clone S, E, and M genes individually from a single codon optimized SEM genetic construct.

**Author Contributions:** Conceptualization, J.C.M., D.F.R., M.A.E., S.R., D.I.G., M.P., J.M.M., E.V., W.R.H. and J.T.; Data curation, J.C.M., S.C., D.F.R., M.A.E., K.C.D., J.R., B.M.T., J.L.M., S.L.G., E.V., W.R.H. and J.T.; Formal analysis, J.C.M., S.C., D.F.R., M.A.E., K.C.D., J.R., B.M.T., J.L.M., S.L.G., E.V., W.R.H. and J.T.; Funding acquisition, C.Y.W., D.I.G., D.H. and J.T.; Investigation, J.C.M., D.F.R., L.E., M.A.E., A.H.Y.Y., J.P.C., K.C.D., J.R., B.M.T., J.L.M., G.D., S.L.G., D.F.J.P., S.A.W., M.P., E.V., W.R.H. and J.T.; Methodology, J.C.M., D.F.R., L.E., M.A.E., A.H.Y.Y., J.P.C., K.C.D., J.R., B.M.T., J.L.M., G.D., S.L.G., D.F.J.P., S.A.W., M.P., E.V., W.R.H. and J.T.; Project administration, C.Y.W. and D.H.; Resources, J.R., S.R., D.F.J.P., M.P., E.V., W.R.H. and J.T.; Supervision, D.F.J.P., J.M.M., E.V., W.R.H. and J.T.; Validation, J.C.M., S.C., D.F.R., M.A.E., K.C.D., J.R., B.M.T., J.L.M., S.L.G., E.V., W.R.H. and J.T.; Writing—original draft, J.C.M., S.C., D.F.R. and J.T.; Writing—review and editing, J.C.M., S.C., D.F.R., M.A.E., D.I.G., J.M.M. and J.T. All authors have read and agreed to the published version of the manuscript.

**Funding:** This work was supported by grants from the National Health and Medical Research Council (NHMRC) Medical Research Future Fund (MRFF) (APP2013957), Avalia Immunotherapies Limited, Wellington, New Zealand, Vaccine Alliance Aotearoa New Zealand, Wellington, New Zealand; JT and DG acknowledge support from the Jack Ma Foundation for parts of the SARS-CoV-2 VLP work in this manuscript. The salary for BMT was supported by an NHMRC Ideas grant awarded to EV, BMT and JT (APP1181580); funding from the Kim Wright Foundation, awarded to EV and JT, is gratefully acknowledged for supporting the establishment of the ALI-HNE model. We acknowledge our public health partners and the Victorian Department of Health and Human Services, the major funder of the Victorian Infectious Diseases Reference Laboratory.

**Institutional Review Board Statement:** The study was conducted in accordance with the Declaration of Helsinki, and study approval was received from the Sydney Children’s Hospital Network Ethics Review Board (HREC/16/SCHN/120) and the Medicine and Dentistry Human Ethics Subcommittee, University of Melbourne (HREC/2057111). The animal study protocol was approved by The Walter and Eliza Hall Institute of Medical Research Animal Ethics Committee (2020.016) and the University of Melbourne Animal Ethics Committee (2020-20198).

**Informed Consent Statement:** Written consent was obtained from all participants (or participants’ guardians) prior to collection of biospecimens.

**Data Availability Statement:** The raw data supporting the conclusions of this article will be made available by the authors on request.

**Acknowledgments:** We thank the Biological Optical Microscopy Platform (BOMP), University of Melbourne for their assistance.

**Conflicts of Interest:** Author Steven Rockman was employed by the company Seqirus. The remaining authors declare that the research was conducted in the absence of any commercial or financial relationships that could be construed as a potential conflict of interest. The funders had no role in the design of the study; in the collection, analyses, or interpretation of data; in the writing of the manuscript; or in the decision to publish the results.

## References

1. Polack, F.P.; Thomas, S.J.; Kitchin, N.; Absalon, J.; Gurtman, A.; Lockhart, S.; Perez, J.L.; Perez Marc, G.; Moreira, E.D.; Zerbini, C.; et al. Safety and Efficacy of the BNT162b2 mRNA COVID-19 Vaccine. *N. Engl. J. Med.* **2020**, *383*, 2603–2615. [[CrossRef](#)]
2. Baden, L.R.; El Sahly, H.M.; Essink, B.; Kotloff, K.; Frey, S.; Novak, R.; Diemert, D.; Spector, S.A.; Rouphael, N.; Creech, C.B.; et al. Efficacy and Safety of the mRNA-1273 SARS-CoV-2 Vaccine. *N. Engl. J. Med.* **2021**, *384*, 403–416. [[CrossRef](#)]
3. Kurhade, C.; Zou, J.; Xia, H.; Liu, M.; Chang, H.C.; Ren, P.; Xie, X.; Shi, P.Y. Low neutralization of SARS-CoV-2 Omicron BA.2.75.2, BQ.1.1 and XBB.1 by parental mRNA vaccine or a BA.5 bivalent booster. *Nat. Med.* **2023**, *29*, 344–347. [[CrossRef](#)] [[PubMed](#)]
4. Qu, P.; Evans, J.P.; Faraone, J.N.; Zheng, Y.M.; Carlin, C.; Anghelina, M.; Stevens, P.; Fernandez, S.; Jones, D.; Lozanski, G.; et al. Enhanced neutralization resistance of SARS-CoV-2 Omicron subvariants BQ.1, BQ.1.1, BA.4.6, BF.7, and BA.2.75.2. *Cell Host Microbe* **2023**, *31*, 9–17.e13. [[CrossRef](#)] [[PubMed](#)]
5. Takashita, E.; Kinoshita, N.; Yamayoshi, S.; Sakai-Tagawa, Y.; Fujisaki, S.; Ito, M.; Iwatsuki-Horimoto, K.; Halfmann, P.; Watanabe, S.; Maeda, K.; et al. Efficacy of Antiviral Agents against the SARS-CoV-2 Omicron Subvariant BA.2. *N. Engl. J. Med.* **2022**, *386*, 1475–1477. [[CrossRef](#)] [[PubMed](#)]
6. Patel, R.; Kaki, M.; Potluri, V.S.; Kahar, P.; Khanna, D. A comprehensive review of SARS-CoV-2 vaccines: Pfizer, Moderna & Johnson & Johnson. *Hum. Vaccines Immunother.* **2022**, *18*, 2002083. [[CrossRef](#)]
7. Sekine, T.; Perez-Potti, A.; Rivera-Ballesteros, O.; Stralin, K.; Gorin, J.B.; Olsson, A.; Llewellyn-Lacey, S.; Kamal, H.; Bogdanovic, G.; Muschiol, S.; et al. Robust T Cell Immunity in Convalescent Individuals with Asymptomatic or Mild COVID-19. *Cell* **2020**, *183*, 158–168.e114. [[CrossRef](#)]
8. Grifoni, A.; Weiskopf, D.; Ramirez, S.I.; Mateus, J.; Dan, J.M.; Moderbacher, C.R.; Rawlings, S.A.; Sutherland, A.; Premkumar, L.; Jadi, R.S.; et al. Targets of T Cell Responses to SARS-CoV-2 Coronavirus in Humans with COVID-19 Disease and Unexposed Individuals. *Cell* **2020**, *181*, 1489–1501.e1415. [[CrossRef](#)]
9. Nguyen, T.H.O.; Rowntree, L.C.; Petersen, J.; Chua, B.Y.; Hensen, L.; Kedzierski, L.; van de Sandt, C.E.; Chaurasia, P.; Tan, H.X.; Habel, J.R.; et al. CD8(+) T cells specific for an immunodominant SARS-CoV-2 nucleocapsid epitope display high naive precursor frequency and TCR promiscuity. *Immunity* **2021**, *54*, 1066–1082.e1065. [[CrossRef](#)]
10. Sette, A.; Crotty, S. Adaptive immunity to SARS-CoV-2 and COVID-19. *Cell* **2021**, *184*, 861–880. [[CrossRef](#)]
11. Ahmed, S.F.; Quadeer, A.A.; McKay, M.R. Preliminary Identification of Potential Vaccine Targets for the COVID-19 Coronavirus (SARS-CoV-2) Based on SARS-CoV Immunological Studies. *Viruses* **2020**, *12*, 254. [[CrossRef](#)]
12. Keating, G.M.; Noble, S. Recombinant hepatitis B vaccine (Engerix-B): A review of its immunogenicity and protective efficacy against hepatitis B. *Drugs* **2003**, *63*, 1021–1051. [[CrossRef](#)]
13. Venters, C.; Graham, W.; Cassidy, W. Recombivax-HB: Perspectives past, present and future. *Expert Rev. Vaccines* **2004**, *3*, 119–129. [[CrossRef](#)]
14. Roy, V.; Jung, W.; Linde, C.; Coates, E.; Ledgerwood, J.; Costner, P.; Yamshchikov, G.; Streeck, H.; Juelg, B.; Lauffenburger, D.A.; et al. Differences in HPV-specific antibody Fc-effector functions following Gardasil(R) and Cervarix(R) vaccination. *NPJ Vaccines* **2023**, *8*, 39. [[CrossRef](#)] [[PubMed](#)]
15. Zaman, K.; Dudman, S.; Stene-Johansen, K.; Qadri, F.; Yunus, M.; Sandbu, S.; Gurley, E.S.; Overbo, J.; Julin, C.H.; Dembinski, J.L.; et al. HEV study protocol: Design of a cluster-randomised, blinded trial to assess the safety, immunogenicity and effectiveness of the hepatitis E vaccine HEV 239 (Hecolin) in women of childbearing age in rural Bangladesh. *BMJ Open* **2020**, *10*, e033702. [[CrossRef](#)] [[PubMed](#)]
16. Zhang, X.; Wei, M.; Sun, G.; Wang, X.; Li, M.; Lin, Z.; Li, Z.; Li, Y.; Fang, M.; Zhang, J.; et al. Real-time stability of a hepatitis E vaccine (Hecolin<sup>®</sup>) demonstrated with potency assays and multifaceted physicochemical methods. *Vaccine* **2016**, *34*, 5871–5877. [[CrossRef](#)] [[PubMed](#)]
17. Nadeem, A.Y.; Shehzad, A.; Islam, S.U.; Al-Suhaimi, E.A.; Lee, Y.S. Mosquirix RTS, S/AS01 Vaccine Development, Immunogenicity, and Efficacy. *Vaccines* **2022**, *10*, 713. [[CrossRef](#)] [[PubMed](#)]
18. Collett, S.; Earnest, L.; Carrera Montoya, J.; Edeling, M.A.; Yap, A.; Wong, C.Y.; Christiansen, D.; Roberts, J.; Mumford, J.; Lecouturier, V.; et al. Development of virus-like particles with inbuilt immunostimulatory properties as vaccine candidates. *Front. Microbiol.* **2023**, *14*, 1065609. [[CrossRef](#)] [[PubMed](#)]
19. Tran, B.M.; Grimley, S.L.; McAuley, J.L.; Hachani, A.; Earnest, L.; Wong, S.L.; Caly, L.; Druce, J.; Purcell, D.F.J.; Jackson, D.C.; et al. Air-Liquid-Interface Differentiated Human Nose Epithelium: A Robust Primary Tissue Culture Model of SARS-CoV-2 Infection. *Int. J. Mol. Sci.* **2022**, *23*, 835. [[CrossRef](#)] [[PubMed](#)]

20. Hierholzer, J.C.; Killington, R.A. Virus isolation and quantitation. In *Virology Methods Manual*; Academic Press: Cambridge, MA, USA, 1996; pp. 25–46.
21. Awatade, N.T.; Wong, S.L.; Capraro, A.; Pandzic, E.; Slapetova, I.; Zhong, L.; Turgutoglu, N.; Fawcett, L.K.; Whan, R.M.; Jaffe, A.; et al. Significant functional differences in differentiated Conditionally Reprogrammed (CRC)- and Feeder-free Dual SMAD inhibited-expanded human nasal epithelial cells. *J. Cyst. Fibros* **2021**, *20*, 364–371. [[CrossRef](#)] [[PubMed](#)]
22. Deliyannis, G.; Gherardin, N.A.; Wong, C.Y.; Grimley, S.L.; Cooney, J.P.; Redmond, S.J.; Ellenberg, P.; Davidson, K.C.; Mordant, F.L.; Smith, T.; et al. Broad immunity to SARS-CoV-2 variants of concern mediated by a SARS-CoV-2 receptor-binding domain protein vaccine. *EBioMedicine* **2023**, *92*, 104574. [[CrossRef](#)]
23. Mach, N.; Gillessen, S.; Wilson, S.B.; Sheehan, C.; Mihm, M.; Dranoff, G. Differences in dendritic cells stimulated in vivo by tumors engineered to secrete granulocyte-macrophage colony-stimulating factor or Flt3-ligand. *Cancer Res.* **2000**, *60*, 3239–3246. [[PubMed](#)]
24. Vremec, D.; Pooley, J.; Hochrein, H.; Wu, L.; Shortman, K. CD4 and CD8 expression by dendritic cell subtypes in mouse thymus and spleen. *J. Immunol.* **2000**, *164*, 2978–2986. [[CrossRef](#)] [[PubMed](#)]
25. Collett, S.; Torresi, J.; Silveira, L.E.; Truong, V.K.; Christiansen, D.; Tran, B.M.; Vincan, E.; Ramsland, P.A.; Elbourne, A. Investigating virus-host cell interactions: Comparative binding forces between hepatitis C virus-like particles and host cell receptors in 2D and 3D cell culture models. *J. Colloid Interface Sci.* **2021**, *592*, 371–384. [[CrossRef](#)] [[PubMed](#)]
26. Bahnan, W.; Wrighton, S.; Sundwall, M.; Blackberg, A.; Larsson, O.; Hoglund, U.; Khakzad, H.; Godzwon, M.; Walle, M.; Elder, E.; et al. Spike-Dependent Opsonization Indicates Both Dose-Dependent Inhibition of Phagocytosis and That Non-Neutralizing Antibodies Can Confer Protection to SARS-CoV-2. *Front. Immunol.* **2021**, *12*, 808932. [[CrossRef](#)]
27. Zhang, A.; Stacey, H.D.; D’Agostino, M.R.; Tugg, Y.; Marzok, A.; Miller, M.S. Beyond neutralization: Fc-dependent antibody effector functions in SARS-CoV-2 infection. *Nat. Rev. Immunol.* **2023**, *23*, 381–396. [[CrossRef](#)]
28. Low, J.S.; Vaqueirinho, D.; Mele, F.; Foglierini, M.; Jerak, J.; Perotti, M.; Jarrossay, D.; Jovic, S.; Perez, L.; Cacciatore, R.; et al. Clonal analysis of immunodominance and cross-reactivity of the CD4 T cell response to SARS-CoV-2. *Science* **2021**, *372*, 1336–1341. [[CrossRef](#)]

**Disclaimer/Publisher’s Note:** The statements, opinions and data contained in all publications are solely those of the individual author(s) and contributor(s) and not of MDPI and/or the editor(s). MDPI and/or the editor(s) disclaim responsibility for any injury to people or property resulting from any ideas, methods, instructions or products referred to in the content.